Article

Design and Parameter Optimization of a Rigid–Flexible Coupled Rod Tooth Threshing Device for Ratoon Rice Based on MBD-DEM

Weijian Liu [1], Xuegeng Chen [1] and Shan Zeng [2],*

[1] Key Laboratory of Modern Agricultural Equipment and Technology, Ministry of Education, Jiangsu University, Zhenjiang 212013, China; 1000005920@ujs.edu.cn (W.L.); 1000005204@ujs.edu.cn (X.C.)

[2] College of Engineering, South China Agricultural University, Guangzhou 510642, China

* Correspondence: shanzeng@scau.edu.cn

Abstract: To solve the problem of the high loss rate of threshing devices during the mechanical harvesting of ratoon rice, we propose a method using the principle of rigid–flexible coupling in this paper to reduce losses. Through analysis of the forces and collisions on ratoon rice grains during the threshing process, it has been confirmed that changing the structure and materials of the threshing contact components can effectively reduce grain loss. A rigid–flexible coupling rod tooth was designed, and the overall structural parameters of the device were determined based on force analysis results and dimensional boundary conditions. The MBD-DEM coupling method was used to simulate the threshing process, and the force conditions of the threshing rod teeth and threshing drum were obtained. The influence of the feeding amount and of the flexible body thickness on the crushing of ratoon rice grains was analyzed. In order to obtain the device's optimal parameter combination, a three-factor quadratic regression orthogonal rotation combination experiment was conducted with drum speed, flexible body thickness, and rod tooth length as experimental factors. The optimization results showed that when the drum speed, flexible body thickness, and rod tooth length were 684 r/min, 3.86 mm, and 72.7 mm, respectively, the crushing rate, entrainment loss rate, and uncleaned rate were 1.260%, 2.132%, and 1.241%, respectively. The bench test showed that it is feasible to use the MBD–DEM coupling method to measure the motion and force of ratoon rice. The rigid–flexible coupling threshing device can reduce the grain crushing rate while ensuring grain cleanliness. Compared with traditional threshing devices, the crushing rate and entrainment loss rate of the rigid–flexible coupling threshing device were reduced by 55.7% and 27.5%, respectively. The research results can provide a reference for the design of threshing devices for ratoon rice harvesters.

Keywords: ratoon rice; threshing device; rigid–flexible coupling; MBD-DEM; test

1. Introduction

The rice crop area in China is about 30 million hectares, with an annual output of more than 210 million tons [1–3]. Ratoon rice has the advantages of being harvested twice after being planted once, making full use of light and temperature resources, increasing grain production and income, and providing good rice quality [4]. Ratoon rice has been rapidly promoted in recent years in suitable areas in the middle and lower reaches of the Yangtze River [5–7]. Threshing is a crucial step in the mechanized harvesting of rice [8,9], where traditional threshing devices use rigid rod teeth. However, the grains of ratoon rice are different from ordinary rice, and ratoon rice grains are more prone to breakage. Therefore, when using traditional threshing devices to process ratoon rice, the phenomenon of grain breakage is significant, seriously reducing yield [10–12].

Scholars have conducted a great deal of research on traditional rice-threshing devices, but there is still no relevant research on low-damage threshing of ratoon rice. Liu Yanbin et al. [13] designed a variable-diameter threshing cylinder using the MBD–DEM

coupling method, improving the operational performance of the threshing drum. However, due to the fact that the research object was ordinary rice and the fragmentation phenomenon is not very severe in ordinary rice compared to ratoon rice, they did not effectively study the damage to ratoon rice grains caused by rod teeth. Wang Xianren et al. [14] studied the effect of rice maturity on the degree of threshing damage. The results showed that immature rice absorbs more energy under external mechanical forces, and the mechanical damage during harvesting is also significant. From an energy perspective, they found that grains are damaged during threshing due to the energy absorbed being greater than that of the rice's crushing limit, but did not propose effective ways to reduce rice grain damage. Xie Fangping [15] conducted experiments on a flexible rod tooth threshing device and studied the threshing mechanism of a flexible rod tooth drum. Based on energy conservation analysis, the stress and deformation of the flexible threshing teeth under impact force were analyzed, but the optimal thickness parameter of the flexible body was not determined.

In summary, the collision and impact between rice plants and the threshing device during ratoon rice threshing are the main causes of grain loss and breakage. Effectively reducing the impact of the threshing device on rice plants can reduce grain loss and breakage during harvesting. This article focuses on the problem of grain loss in the threshing system of a ratoon rice harvester. By analyzing the grain shedding process during the threshing collision process, an improved scheme is proposed using a rigid–flexible coupling structure to reduce the force of grain collisions. MBD–DEM coupling is used to simulate the threshing process, and the parameters of the buffer mechanism and flexible surface are optimized to provide a theoretical reference for reducing grain loss during ratoon rice harvesting.

2. Force Analysis of Threshing Process

2.1. Grain Stress Analysis

Figure 1 shows the force exerted on ratoon rice grains when the ratoon rice plant comes into contact with rod teeth. Due to the orderly arrangement of these grains, the contact force between different columnar grains can be neglected when the direction of force is aligned with the stem axis. If the grains come into contact with the rod teeth, they are subjected to pressure p_1 along the stem direction, shear force s_1 perpendicular to the stem direction, rod tooth pressure n_1, and pressure q_2 from adjacent grains. A sub-coordinate system ox_1y_1 is established along the stem direction; n_1 can be decomposed into n_{1x} and n_{1y} and q_2 can be decomposed into q_{2x} and q_{2y}. If a ratoon rice grain is not in contact with the rod teeth, it is subjected to tensile force t_n in the direction of the grain stem, shear force s_n in the direction perpendicular to the grain stem, pressure q_{n-1} from the adjacent grains below, and pressure q_{n+1} from the adjacent grains above. In the coordinate system ox_ny_n, q_{n-1} and q_{n+1} can be decomposed into $q_{(n-1)x}$, $q_{(n-1)y}$, and $q_{(n+1)x}$, $q_{(n+1)y}$.

Assuming that the limit of compression in the direction of the grain stem for a single ratoon rice grain is p_L (Unit: N), the limit of tension in the direction of the grain stem is t_L (Unit: N), and the limit of shear in the direction perpendicular to the grain stem is s_L (Unit: N). If the ratoon rice grains come into contact with the rod teeth, the mechanical principle of the detached ratoon rice grains is expressed by the following equation:

$$\begin{cases} n_{1x} - q_{2x} - \mu q_{2y} > p_L \\ n_{1y} - q_{2y} > s_L \end{cases} \tag{1}$$

In the formula, μ represents the sliding friction coefficient between ratoon rice grains.

If the ratoon rice grains do not come into contact with the rod teeth, the mechanical principle of the detached ratoon rice grains is expressed by the following equation:

$$\begin{cases} q_{(n-1)x} + q_{(n+1)x} - \mu q_{(n-1)y} - \mu q_{(n+1)y} > t_L \\ q_{(n-1)y} - q_{(n+1)y} > s_L \end{cases} \tag{2}$$
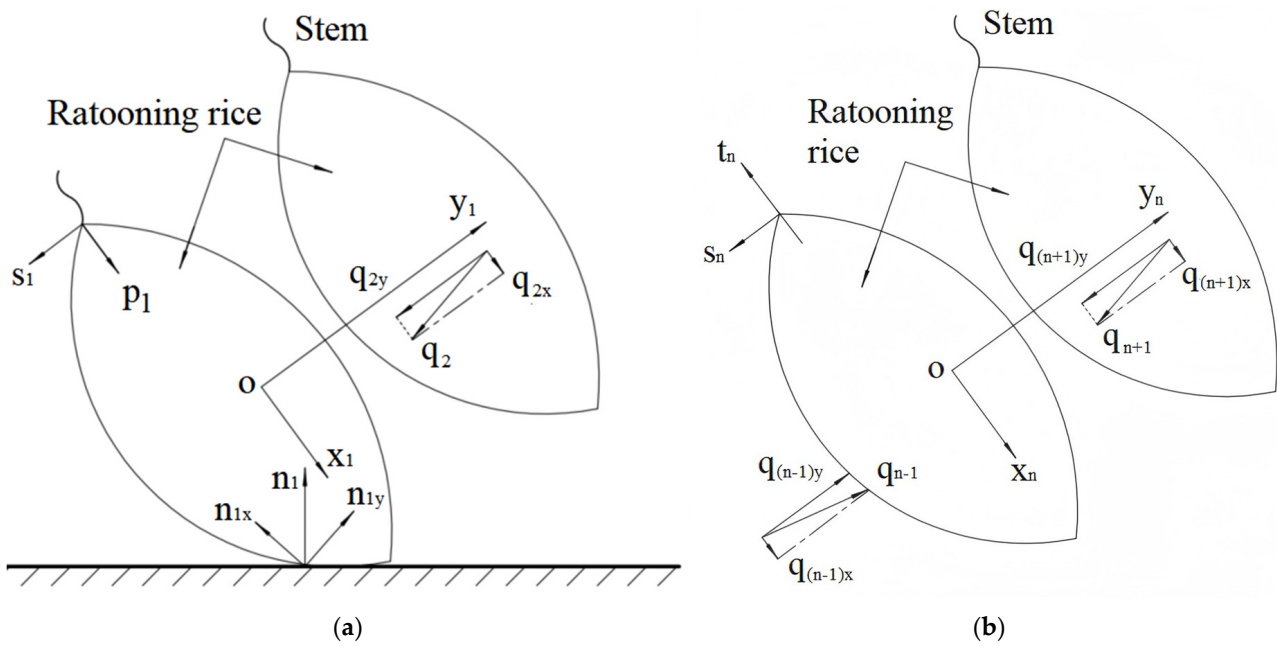
Figure 1. Schematic diagram of grain stress. (**a**) Ratoon rice grains in contact with rod teeth; (**b**) ratoon rice grains with no contact with the rod teeth. Note: s_1 is the shear force of the stem on ratoon rice grains, N; p_1 is the pressure exerted by the stem on the ratoon rice grains, N; ox_1y_1 is the floating coordinate system; n_1 is the impact force of the rod teeth on the grain, N; n_1x is a component of n_1 in the direction of x_1, N; n_{1y} is a component of $n1$ in the direction of y_1, N; q_2 is the interaction force between adjacent grains, N; q_{2x} is a component of q_2 in the direction of x_1, N; q_{2y} is a component of q_2 in the direction of y_1, N; s_n is the shear force of the stem on ratoon rice grains, N; t_n is the tensile force of the stem on the grain, N; ox_ny_n is the floating coordinate system; q_{n-1} is the pressure from the ratoon rice grains below, N; $q_{(n-1)x}$ is a component of q_{n-1} in the direction of x_n, N; $q_{(n-1)y}$ is a component of q_{n-1} in the direction of y_n, N; q_{n+1} is the pressure from the ratoon rice grains above, N; $q_{(n+1)x}$ is a component of q_{n+1} in the direction of x_n, N; $q_{(n+1)y}$ is a component of q_{n+1} in the direction of y_n, N.

2.2. Collision Process Analysis

During the threshing process, the threshing drum rotates at a high speed, and the collision between rice plants and rod teeth is completed in an instant. Therefore, the threshing process can be regarded as a collision process of a mass point. Treating ratoon rice grains as a mass point, the collision process can be expressed as:

$$P = \int_{t_0}^{t_0 + \Delta t} ma(t)dt \tag{3}$$

where P is the impulse received by the ratoon rice grain, N·s; m is the mass of the ratoon rice grain, kg; a is the acceleration, m/s^2; and t is the time, s.

When a collision occurs, a huge contact impact force appears instantly. When the external impulse remains constant, there is a significant relationship between the peak impact force and the length of the collision time. Extending the collision time can significantly reduce the peak collision acceleration, thereby reducing the impact force at the moment of contact and reducing the grain breakage caused by collisions [16]. Starting from the moment when the ratoon rice grains come into contact with the rod teeth, this process can be simplified as a forward collision problem between the constrained mass and the elastic wall, as shown in Figure 2.
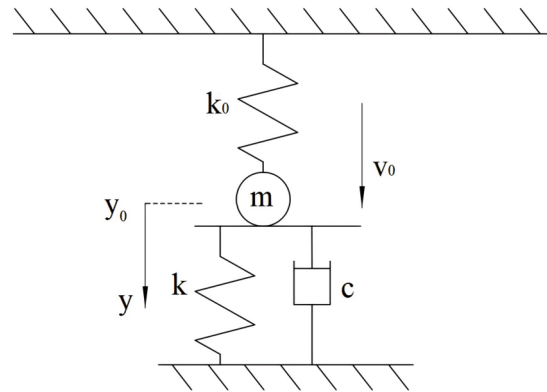
Figure 2. Simplified model of stress on ratoon rice grains during collision. Note: v_0 is the initial velocity when the ratoon rice grain collides with the rod teeth, m·s^{-1}; c is the damping coefficient of the system, N·s ·m^{-1}; k is the stiffness coefficient of the rod teeth, N·m^{-1}; k_0 is the stiffness coefficient of the ratoon rice grains, N·m^{-1}; m is the mass of the ratoon rice grains, g; y_0 is the initial point of collision; and y is the initial velocity direction of ratoon rice grains.

During the collision process, the motion equation of a single-degree-of-freedom system is:

$$\begin{cases} m\ddot{y} + c\dot{y} + (k + k_0)y = ky_0 \\ y(0) = y_0 \\ \dot{y}(0) = v_0 \end{cases} \tag{4}$$

In the case of insufficient damping, the solution to Equation (4) is:

$$y = Ae^{-\varsigma\omega_n t}\sin\omega_d t + \frac{k}{k + k_0}y_0 \tag{5}$$

When the initial displacement is 0, the collision time can be determined by the minimum positive root of Formula (6):

$$f(t) = c\dot{y} + k(y - y_0) = 0 \tag{6}$$

The following can be obtained:

$$Ae^{-\zeta\omega_n\Delta t}\left\{\left[k_0 - \left(1 - 2\zeta^2\right)\omega_n{}^2\right]sn - 2\zeta\omega_n\omega_d cs\right\} + \frac{kk_0}{k + k_0}y_0 = 0 \tag{7}$$

In this formula:

$$\begin{aligned} \varsigma &= \frac{c}{2m\omega_n} \\ sn &= \sin\omega_d\Delta t \\ cs &= \cos\omega_d\Delta t \\ A &= \frac{\frac{v_0}{\omega_d}}{\frac{\zeta}{\sqrt{1-\zeta^2}}\sin\phi + \cos\phi} \\ \omega_d &= \sqrt{1 - \zeta^2}\,\omega_n \\ \omega_n &= \sqrt{\frac{k + k_0}{m}} \end{aligned} \tag{8}$$

where ζ is the viscous damping ratio, $\zeta < 1$; A is the amplitude, mm; ω_d is the damped natural frequency, Hz; and ω_n is the undamped natural frequency, Hz.

The collision time can be calculated using the following formula:

$$\Delta t = \frac{\pi + \arctan\lambda_2}{\omega_n\sqrt{1 - \zeta^2}} \tag{9}$$

In this formula:

$$\lambda_2 = \frac{2\zeta\sqrt{1-\zeta^2}}{k_0/\omega_n^2 - (1-2\zeta^2)} \tag{10}$$

From Equations (9) and (10), it can be seen that the collision time is related to the inherent parameters of the system, such as the stiffness coefficient, mass, and damping coefficient, and is independent of the initial collision velocity. However, the stiffness and damping coefficients of the system depend on its materials and structure. Therefore, by changing the structure and contact materials of the collision system, the stiffness coefficient of the system can be reduced and the damping coefficient can be increased, thereby reducing the natural frequency of the system, increasing the viscous damping ratio of the system and effectively prolonging the collision contact time. When the collision impulse is constant, extending the collision time can reduce the peak force on the ratoon rice grains, thereby reducing the probability of the ratoon rice grains being crushed by the rod teeth.

3. Structure Design and Working Principles

3.1. Overall Structure and Working Principle

Based on the analysis of the force and collision model of ratoon rice grains, in order to reduce the crushing rate of ratoon rice grains, the threshing device needs to be designed in such a way to increase the damping coefficient and reduce the stiffness coefficient. Therefore, in this work, we designed a flexible striking mechanism with polyurethane rubber as the direct contact material. The structure of the threshing device is shown in Figure 3.


(**a**)

(**b**)
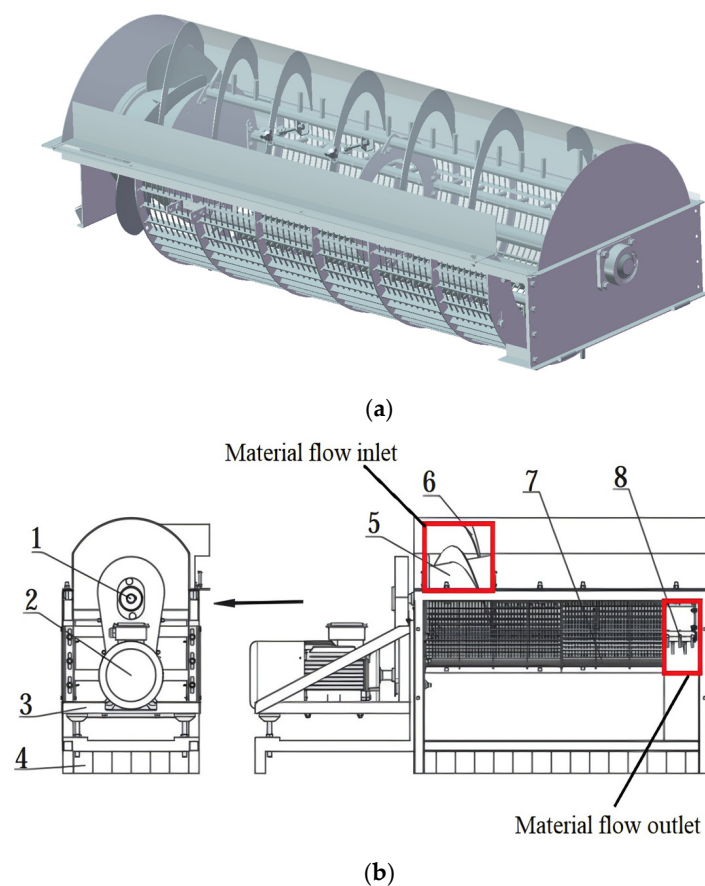
Figure 3. Overall structure of the device. (1) Transmission structure; (2) motor; (3) motor adjustment bracket; (4) splice box; (5) threshing drum; (6) flow guide; (7) concave screen; (8) threshing rod teeth. (**a**) Three-dimensional model of threshing device; (**b**) Two-dimensional model of threshing device.

The rigid–flexible coupling threshing device mainly consists of a threshing drum, a concave plate screen, a drum cover plate, etc. Its working mode is longitudinal flow, and the threshing process can be divided into four stages, namely, feeding, threshing, separating, and discharging of rice plant stems [17]. The ratoon rice plants enter the threshing chamber under the forced action of the spiral feeding device, and under the joint action of the threshing rod teeth and the guide bar, they move backwards along the axial direction in a spiral motion [18]. During this process, the ratoon rice falls off from the rice ear under the impact and collision of the rod teeth and the concave sieve, completing the threshing process [19]. The detached rice grains and some impurities enter the cleaning device, and the remaining impurities, such as long stems, move to the end of the drum under the action of the guide rod and then discharge outside the device.

3.2. Determination of the Threshing Device's Main Parameters

The rigid–flexible coupling threshing drum is composed of a spiral feeding device, rigid–flexible coupling rod teeth, spoke rods, spoke plates, and drum shafts. It can be divided into a feeding section, a threshing section, and an impurity section along the drum axis (Figure 4).
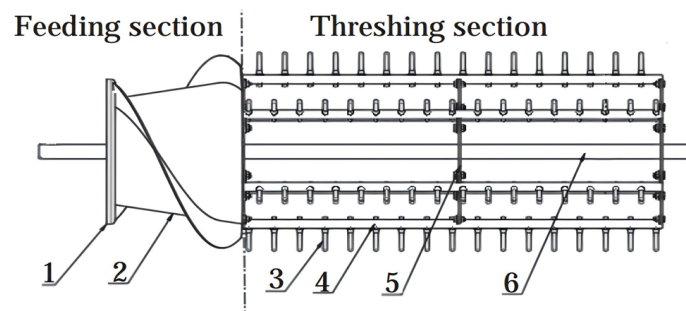
Figure 4. The structure diagram of threshing device. (1) Fender; (2) spiral feeding device; (3) rigid-flexible coupling rod teeth; (4) spoke rod; (5) spoke plate; (6) drum shaft.

3.2.1. Spiral Feeding Device

The spiral feeding device enhances the flow ability of rice plants and prevents blockage of the drum feeding inlet. The force analysis of the rice plants fed into the feeding device is shown in Figure 5. Through the analysis, it can be concluded that the frictional force F_f between the spiral blade and the rice plants is the component force in the radial movement of the rice plants. F_f and the normal thrust of the spiral blades on the rice plants form a combined force F, which drives the axial flow of the rice plants. To ensure the fluidity of rice plant feeding and avoid blockage, the axial conveying force should be greater than the axial resistance, as follows:

$$\begin{cases} T\cos\beta = F_f\sin\beta \\ T\tan\alpha = F_f \end{cases} \tag{11}$$

where T is the normal thrust of the spiral blade on the rice plants, N; F_f is the friction force between the spiral blade and the rice plants, N; α is the friction angle between the rice plants and the spiral blade, °; and β is the spiral blade helix angle, °.

According to Equation (11), the conditions for ensuring the axial flow of ratoon rice plants is $\beta > 90°-\alpha$. β affects the axial feeding speed of the rice plants and the power consumption of the spiral feeding device. The higher the feeding speed, the faster the rice plants enter the threshing drum and the higher the threshing efficiency. Therefore, under the same rotational speed conditions, the larger the spiral blade helix angle, the smaller the axial thrust generated. On the contrary, the greater the axial thrust generated, the higher the power consumption. Under these conditions, the power distributed by the harvester to the conveying groove decreases, and a large feeding amount can easily cause blockage of the conveying groove. In this device, $\beta = 30°$.
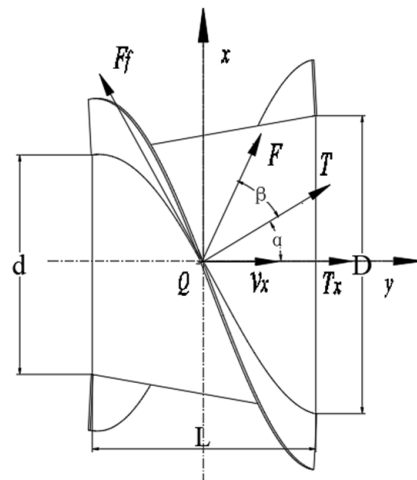
Figure 5. Analysis of stress on rice plants. Note: d is the front section's diameter, mm; L is the length of the screw feed head, mm; D is the diameter of the rear end, mm; v_x is the axial feeding speed of rice plants, kg/s; and T_x is the axial thrust.

The length of the spiral feeding head L is:

$$L = \frac{H}{K} \tag{12}$$

where H is the lead of the spiral blade, mm; and K is the number of spiral heads.

When the lead of the spiral blade H is 600 mm and the number of spiral heads K is 2, the length of the spiral feeding head L is 300 mm. According to the Agricultural Machinery Design Manual [20], the front diameter d is 300 mm, and the rear diameter D is 400 mm.

According to the material characteristics of ratoon rice, the threshing drum element adopts comb brush rod teeth, which has a good threshing effect on ratoon rice with a high moisture content. The production efficiency formula of the threshing device is [20]:

$$z \geq \frac{(1 - R)q}{0.6 q_d} \tag{13}$$

where z is the number of threshing rod teeth; R is the proportion of ratoon rice, %; q is the feeding amount of the threshing device, kg/s; and q_d is the threshing capacity of each rod tooth.

According to Equation (13), it can be calculated that z $\geq$ 99. The calculation formula for the length of the threshing drum l is:

$$l = a\left(\frac{z}{K} - 1\right) + 2\Delta l \tag{14}$$

where a is the tooth trace distance, mm; z is the number of threshing rod teeth; and Δl is the distance between the end rod teeth and the end of the spoke rod, mm.

According to Equation (5), when Δl = 45 mm, the length of the threshing drum is 990 mm.

3.2.2. Design of Threshing Drum Rod Teeth

According to the material characteristics of ratoon rice, high grain moisture content can lead to easy breakage of grains during the threshing process. Therefore, the rigid–flexible coupling rod tooth surface designed in this study is wrapped with polyurethane rubber with a thickness of 2–6 mm [21]. Polyurethane rubber can absorb energy and reduce vibration, reducing their impact on grains. To verify the threshing effect of the rigid–flexible coupling rod teeth, a comparative experiment of three types of rod teeth was designed, as shown in Figure 6. In the simulation, RecurDyn's MFBD (Multi Flexible Body Dynamics)

technology was used to accurately establish a rod tooth simulation model. The three types of rod tooth parameters are as follows: the diameter of the rigid rod teeth is 20 mm; the flexible rod teeth are completely composed of polyurethane rubber and have a diameter of 20 mm; and the rigid–flexible coupling rod teeth have a diameter of 24–32 mm, according to the thickness of the rubber wrapped around them. The length of all three types of rod teeth is set to 70 mm.
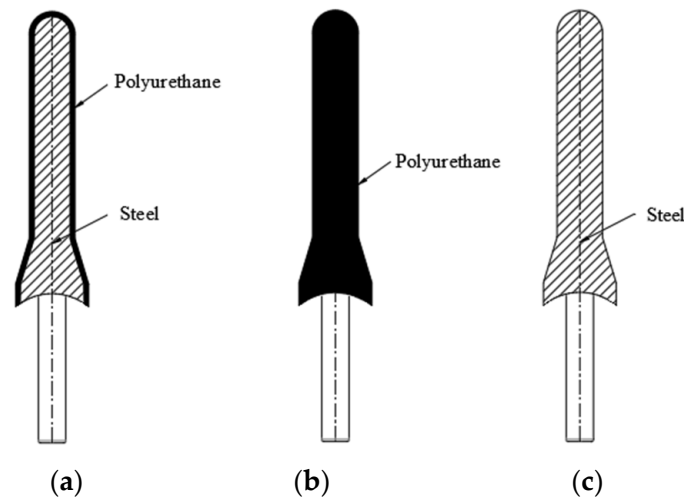
Figure 6. The structure diagrams of three rod teeth. (**a**) Rigid–flexible coupling teeth; (**b**) flexible teeth; (**c**) rigid teeth.

3.2.3. Design of Threshing Device Cover Plate

The cover plate is located at the top of the threshing chamber, with a radius of 330 mm, and there is a guide strip designed inside the cover plate to control the direction of rice plant movement. In order to ensure the fluidity of rice plants in the threshing chamber, a 23° angle is used for the guide strip, and there should be a certain overlap area between the guide strips, as shown in Figure 7.
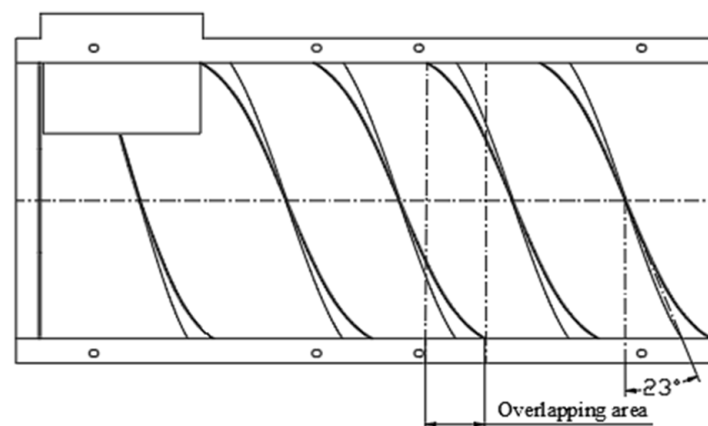
Figure 7. Structure diagram of the threshing device cover plate.

3.2.4. Design of Concave Plate Sieve

The sieve holes of the concave plate sieve are composed of steel wires and flat steel. The threshing performance of different harvesters is set according to the feeding amount. This device sets the sieve hole length to 20 mm, the width to 15 mm, and the concave plate sieve radius to 280 mm. Its structure is shown in Figure 8.
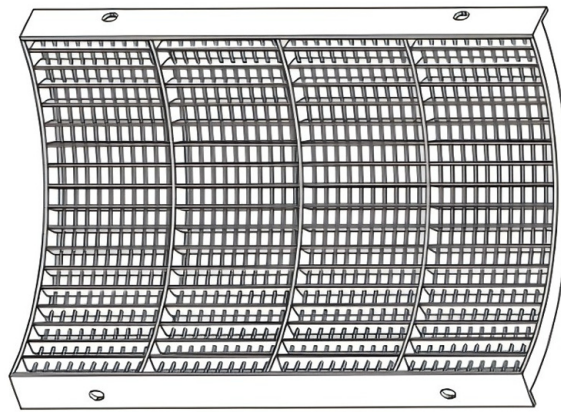
Figure 8. Structure diagram of concave plate sieve.

4. MBD-DEM Coupled Simulation

4.1. Establishment of Mathematical Models

The principle of threshing mainly relies on the impact and friction of the rod teeth on ratoon rice plants. During the threshing process, the rod teeth are subjected to the combined action of pressure P generated by straw compression and frictional force f_s along the tangent direction of the straw teeth. The pressure P caused by the accumulation of straw in the threshing device is calculated by the following formula:

$$P = nB\left(\frac{R_{\max}}{R}\right)^{y} \tag{15}$$

where B is the stacking coefficient; n is the number of teeth rod; R_{max} is the thickness of fluffy straw, mm; and R is the thickness of compressed straw after stacking, mm.

The R_{max} and B can be calculated using Formula (17):

$$\begin{aligned} R_{\max} &= \frac{q}{\rho v w} \\ B &= \frac{n(R_{\max} - R)}{P} \end{aligned} \tag{16}$$

where q is the rate at which ratoon rice plants enter the device, kg/s; ρ is the density of ratooning straw, kg/m^3; v is the movement speed of the ratoon rice plant, m/s; and w is the width of the concave plate, mm.

4.2. Particle Model Establishment

The discrete element method (DEM) has been widely applied in agricultural engineering in recent years [22–26]. The separation process of ratoon rice grains in the threshing device is a nonlinear and uncertain process. In order to study the process of detaching rice grains from ratoon rice plants, a bonded-particle straw model (BSM) with hollow flexible cylindrical bonds was used to establish a ratoon rice plant model, simulating the dynamic behavior of particles under impact, fragmentation, and multiple interaction conditions. In order to improve the computational efficiency and reduce the computational complexity, leaves and fine ears were not considered in the model and the cross-sectional area and structure of straw were assumed to be uniform. The particle factory is located at the feeding inlet of the device, and the particle generation position is randomly selected. The feeding amount is set to 5.0 kg/s. To accurately reproduce the actual feeding situation, the initial particle velocity is set to 5 m/s. Based on the actual dimensions of ratoon rice and straw, the shape of ratoon rice can be simplified to an elliptical sphere, with a long axis of 8.8 mm and a short axis of 3.0 mm, while short straw can be seen as a cylinder with a length of 35–70 mm and a circular cross-sectional radius of 2 mm. The established model is shown in Figure 9.

(**a**)

(**b**)
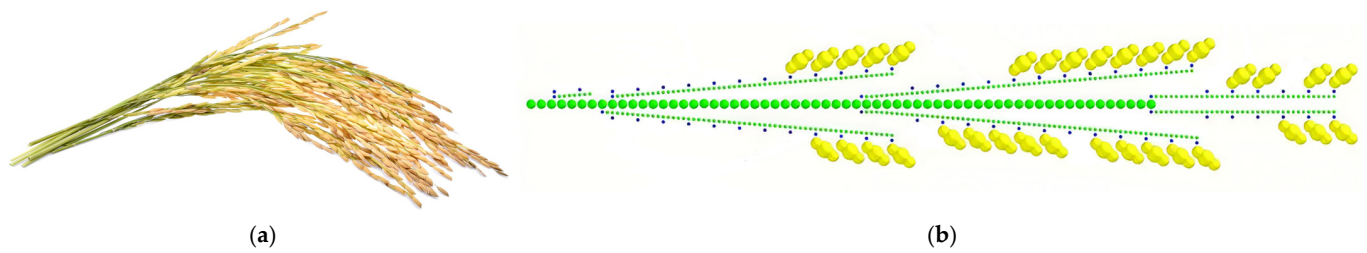
Figure 9. Model establishment. (**a**) Ratooning rice plants; (**b**) ratoon rice plant EDEM model.

The mechanical properties of ratoon rice and short straw were investigated, and the contact coefficients between ratoon rice, short straw, and the device were determined. The results are shown in Tables 1 and 2.

Table 1. Simulation parameter settings.

Item	Poisson's Ratio	Shear Modulus/(Mpa)	Density/(kg·m^{-3})
Ratoon rice	0.30	26	1300
Short straw	0.40	10	100
Polyurethane	0.28	0.027	1072
Threshing device	0.30	70,000	7800

Table 2. Contact coefficients in EDEM.

Item	Restitution Coefficient	Static Friction Coefficient	Rolling Friction Coefficient
Grain-grain	0.2	1.0	0.03
Grain-short straw	0.2	0.8	0.02
Grain-threshing device	0.5	0.58	0.04
Short straw-short straw	0.2	0.90	0.01
Short straw-threshing device	0.2	0.8	0.02
Grain-polyurethane	0.4	0.5	0.01
Short straw-polyurethane	0.35	0.4	0.05

4.3. Analysis of Simulation Results

4.3.1. The Impact Force on the Rod Teeth

Compared with bench tests, simulation can easily obtain the movement process and force situation of straw and ratoon rice in the threshing chamber. In order to verify the consistency between the simulation results and the actual results and to analyze the impact force on the rod teeth and threshing drum, simulation of MBD–DEM coupling was conducted. The simulation process is shown in Figure 10 and lasts for 15 s. From Figure 10, it can be seen that the ratoon rice plants enter the threshing device through the feeding inlet in front of the device. After entering the threshing device, the material is fed through the spiral feeding device on the threshing drum and guided by the top plate to complete the threshing process. Under the high-speed impact of the teeth, the ratoon rice grains fall into the collection box below, and the straw is discharged into the straw collection box behind under the guidance of the top cover. For ease of expression, the rod teeth on the threshing drum are numbered, with three teeth forming a group and a total of six groups. From the inlet to the outlet of the threshing drum, these groups are numbered 1, 2, 3, 4, 5, and 6. Due to the small volume of ratoon rice grains, it is difficult to obtain the force situation of all ratoon rice grains. Ratoon rice grains are in direct contact with the rod teeth. Therefore, by analyzing the force situation of the rod teeth on the threshing drum, the force situation of ratooning grains can be obtained. The normal and tangential average impact forces of the three types of rod teeth on ratoon rice grains were compared and analyzed at drum

speeds of 650, 750, and 850 r/min. The results are shown in Table 3. To facilitate intuitive representation, the data are plotted as a line graph, as shown in Figure 11.

(**a**)   (**b**)
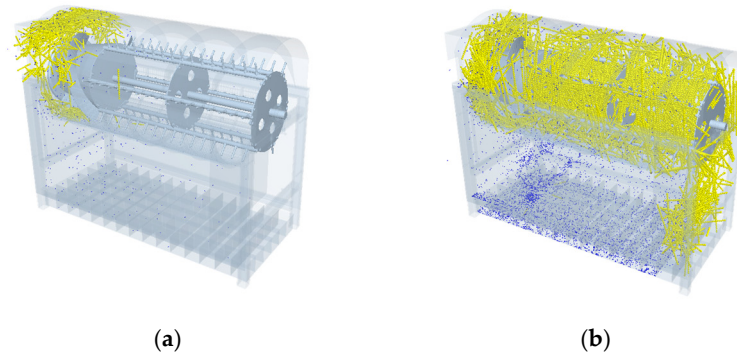
Figure 10. Threshing process simulation. (**a**) Ratoon rice plants have just entered the threshing device. (**b**) Threshing device is filled with material. Note: the blue color in the figure represents ratoon rice grains, and the yellow color represents straw.

Table 3. Simulation result.

| Item	Group	Rigid Rod Teeth			Flexible Rod Teeth			Rigid–Flexible Coupling Rod Teeth		
Threshing drum speed/(r/min)	/	650	750	850	650	750	850	650	750	850
	1	313.57	338.45	342.78	208.74	211.37	209.57	258.53	285.12	298.64
	2	345.48	361.12	357.54	227.36	230.21	235.63	267.73	293.34	321.51
Average normal impact force/N	3	376.83	387.64	402.06	256.80	253.07	272.62	289.04	312.84	356.32
	4	389.38	414.77	417.12	273.46	278.53	276.23	319.30	333.83	368.77
	5	372.82	383.42	415.43	270.33	268.63	275.84	292.64	308.22	345.15
	6	325.51	358.33	386.12	264.31	253.27	268.34	275.23	286.75	337.66
	1	103.87	110.62	121.35	83.66	82.14	85.73	89.72	93.68	99.52
	2	117.16	128.72	126.56	96.32	100.18	115.52	104.73	107.56	117.68
Average tangential impact force/N	3	124.81	131.27	139.50	105.30	110.64	117.31	118.28	117.38	121.64
	4	132.68	138.83	145.83	113.77	121.36	126.84	122.92	125.37	135.56
	5	123.57	130.73	133.63	107.32	116.64	121.38	118.80	121.83	128.52
	6	106.33	126.03	130.88	76.85	86.68	83.54	86.75	98.42	111.16
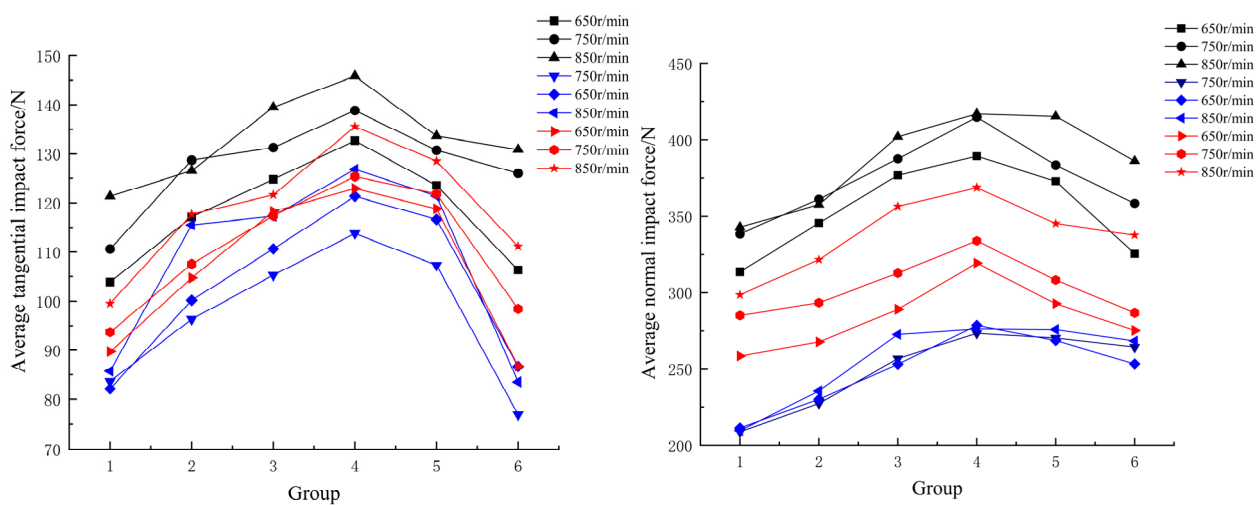
Figure 11. The impact force on the rod teeth. Note: rigid rod teeth: black line; flexible rod teeth: blue line; rigid–flexible coupling rod teeth: red line.

Overall, the normal and tangential impact forces of rigid rod teeth and rigid–flexible coupling rod teeth on ratoon rice grains increase rapidly with an increase in drum speed,

while flexible rod teeth exhibit different phenomena. As the threshing drum speed increases, the increase in the impact force on flexible rod teeth is very small, and some flexible rod teeth show a negative growth trend. This is because there is no rigid body inside the flexible rod teeth. With the increase in threshing drum speed, the flexible body's rod teeth deform. When the speed is too high, the flexible body's rod teeth may even tilt to one side, and at this time, the tilted rod teeth no longer have any threshing ability. From Figure 11, it can also be observed that at the same rotational speed, the normal and tangential impact forces of flexible rod teeth on ratoon rice grains are lower than those of rigid rod teeth, and the impact force on rigid–flexible coupled rod teeth is between the two. After counting the ratoon rice grains under the threshing device, it was found that the entrainment loss rate of flexible rod teeth was significantly higher than that of rigid rod teeth and rigid–flexible coupling rod teeth. This is because the impact force of flexible rod teeth on plants is too small, resulting in incomplete threshing.

4.3.2. Analysis of Ratoon Rice Grain Distribution

To study the threshing effect of each position of the threshing drum, 90 collection boxes were placed below the threshing drum in a 15 × 6 manner. After reaching a stable feeding state, the number of ratoon rice grains in each collection box was counted, and a three-dimensional distribution projection map was drawn, as shown in Figure 12.
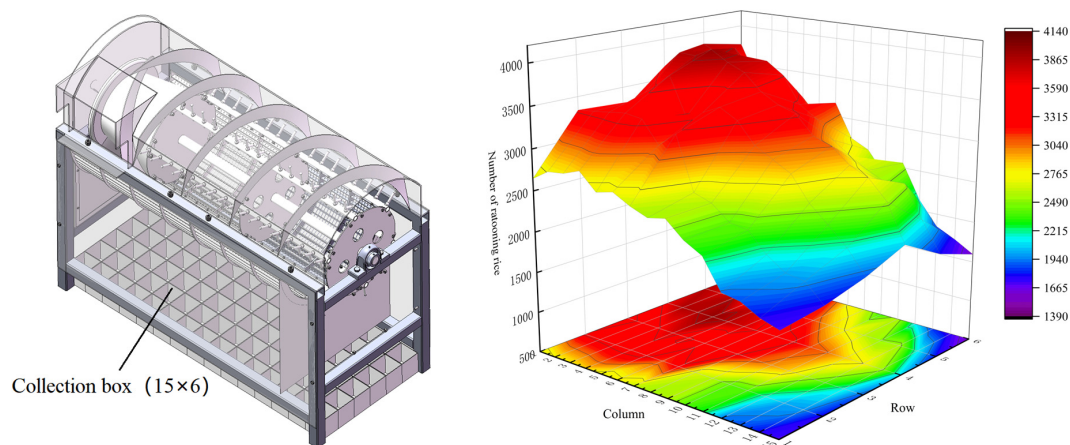

Figure 12. Distribution of ratoon rice grains in the collection box.

Comparing the actual device diagram and the projection diagram in Figure 12, it can be seen that the upper left corner of the projection diagram corresponds to the direction of the material inlet, and the lower right corner of the projection diagram corresponds to the direction of the material outlet. From the three-dimensional distribution map, it can be seen that the distribution of ratoon rice grains in the collection box is not uniform and does not present a perfect axisymmetric distribution state. Overall, the number of ratoon rice grains decreases from the material inlet to the material outlet and increases from the left side of the device to the right side (the feeding inlet side is referred to as the left side). The peak position of the number of particles appears on the right side of the inlet, reaching 4100. The rightward peak position is caused by the rotation of the threshing drum, which rotates clockwise. Most of the separated ratoon rice grains collide with the right inner wall of the device under the impact of the teeth and fall into the collection box below. However, from the distribution status of ratoon rice grains, the number of ratoon rice grains in the collection box on the far-right column is lower than that in the second column on the right. This is due to the bouncing effect of ratoon rice grains, and the number of ratoon rice grains on the side closer to the wall is actually less. The collection box with the least number of particles is located on the right rear side of the device. The number of ratoon rice grains in the collection box is 1597. The small number of particles indicates that the ratoon rice plants at this position have basically completed threshing. The main threshing work has

been completed in the front middle of the drum, and the designed length of the threshing drum meets the requirements. A cleaning device is installed below the threshing drum on the ratoon rice harvester. The distribution of the ratoon rice grains is beneficial for the next cleaning operation and also helps to reduce the grain loss rate. From this analysis, it can be seen that the distribution status of ratoon rice grains is consistent with actual experience, indicating that using EDEM to simulate the threshing process of ratoon rice is feasible.

4.3.3. The Influence of Flexible Body Thickness on Threshing

The force variation curve of the rigid–flexible coupling rod teeth over time is shown in Figure 13. The simulation lasts for 15 s, with the drum speed set to 750 r/min. At the beginning of the simulation, the impact force fluctuates greatly. At this point, the ratoon rice plants have just entered the threshing device and are relatively fluffy. The centrifugal force of the rod teeth is partially offset by the fluffy ratoon rice plants. Meanwhile, the number of ratoon rice plants in the device is relatively small, and the movement height of ratoon rice plants is highly random. The repeated impact of the teeth on the ratoon rice plants, which are moving at a high speed, causes significant fluctuations in the impact force on the teeth. As time goes by, the amount of ratoon rice plants entering the device continues to increase, and the force on the rod teeth also increases. When the simulation time reaches 6 s, a large number of ratoon rice plants have entered the threshing device, which is filled with material. The ratoon rice plants are compressed and become dense, and the teeth of the rod constantly come into contact and collide with the rice plants. The force on the teeth continues to increase, resulting in a high average impact force on the ratoon rice grains, which gradually stabilizes. At this point, the efficiency of the threshing drum reaches its maximum, and a large amount of ratoon rice grains are separated from the plants. Straw is continuously discharged from behind the threshing device, and ratoon rice grains fall into the collection box below.
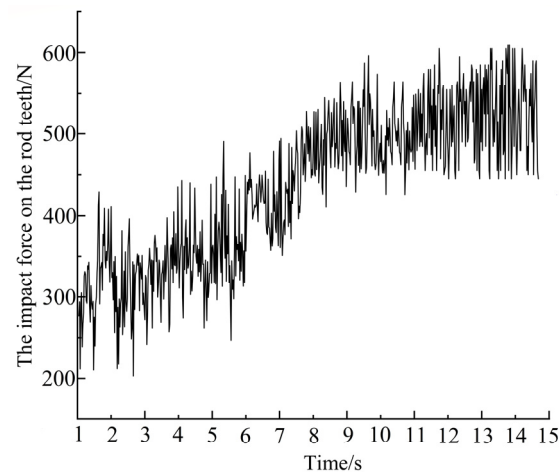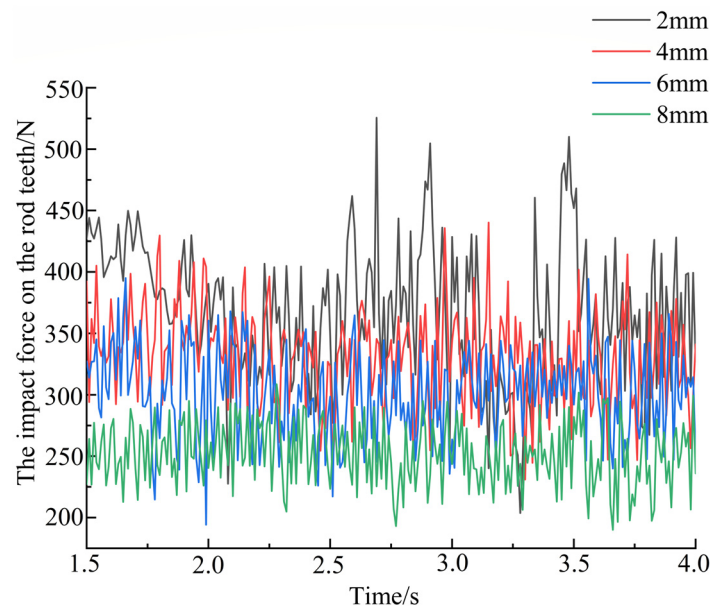

Figure 13. Force fluctuation diagram of rod teeth.

According to the simulation experiment, we used the simulation results after 6 s to analyze the influence of flexible body thickness on the impact force of rod teeth, as shown in Figure 14.

When the feeding rate is relatively stable at 5 kg/s, the thickness of the flexible body increases from 2 mm to 4 mm, 6 mm, and 8 mm, and the average impact force on the rod teeth is 387 N, 368 N, 339 N, and 258 N, respectively. The impact force curve on the rod teeth is shown in Figure 14. From Figure 14, it can be seen that as the thickness of the flexible body increases, the impact force on the teeth decreases continuously. When the thickness of the flexible body reaches 8 mm, the average impact force is the smallest and the fluctuation is also the smallest. An impact force that is too weak prevents the threshing drum from functioning properly, since the rod teeth need to be overloaded stable to an certain extent. Otherwise, the rod teeth will lose their threshing ability and eventually

block the threshing drum. When the blockage is severe, the rod teeth may even deform. It can be seen that the flexible body is too thick to meet the threshing requirements.


Figure 14. Force fluctuation diagram of rod teeth under different flexible body thicknesses.

5. Bench Test

5.1. Test Materials

The experiment was conducted at the Zengcheng Teaching Experimental Base of South China Agricultural University. The basic parameters of the ratoon rice were as follows: plant length, 650–800 mm; thousand-grain weight, 21.85 g; flexible body thickness, 2–6 mm; stem moisture content, 77.56%; grass-to-grain ratio, 1.38. The test bench includes a Y2EJ-160L-4P-15kW-B33 AC motor (2.2 kw 40 axis), an Inspur FE550 AC motor frequency converter (100-240V7-3.5A/50 Hz/550 W), a Shenzhen Tengfei parallel conveyor belt (PVC), a Chengdu Beisaike Instrument XH30001 electronic balance (with an accuracy of 0.001 g), and a Shanghai Shangyi SN-SH-10A moisture measuring instrument. The threshing device bench is shown in Figure 15.
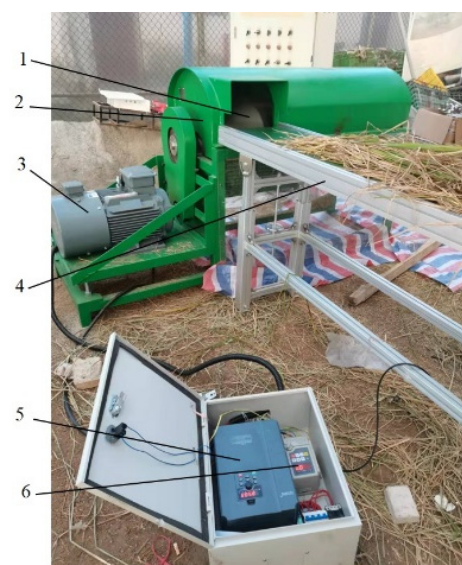
Figure 15. Threshing performance test. (1) Threshing drum. (2) Bench. (3) Motor. (4) Conveyor. (5) Motor inverter. (6) Conveyor belt inverter.

5.2. Evaluation Indicators

The evaluation indicators include the following: crushing rate, Y_1; entrainment loss rate, Y_2; uncleaned rate, Y_3. The calculation method is as follows:

$$\begin{cases} Y_1 = \frac{m_k}{M_1} \times 100\% \\ Y_2 = \frac{m_l}{m_l + M_2} \times 100\% \\ Y_3 = \frac{m_c}{m_c + M_3} \times 100\% \end{cases} \quad (17)$$

where Y_1, Y_2, and Y_3 are the crushing rate, entrainment loss rate, and uncleaned rate, respectively, %; m_k is the mass of crushed ratoon rice, g; M_1 is the total mass of ratoon rice, g; m_1 is the mass of ratoon rice outside the threshing room, g; M_2 is the total mass of ratoon rice in the threshing room, g; m_c is the mass of grains left on the plant after threshing, g; and M_3 is the total mass of detached ratoon rice, g.

5.3. Quadratic Regression Orthogonal Rotation Combination Experiment

Selecting the drum speed, flexible body thickness, and rod tooth length—which all have a significant impact on threshing performance—as experimental factors, a three-factor quadratic regression orthogonal rotation combination experiment was conducted. The crushing rate, entrainment loss rate, and uncleaning rate were used as evaluation indicators, and an average was obtained by repeating each experiment three times. The experimental factor codes and results are shown in Tables 4 and 5, and the analysis of variance is shown in Table 6. X_1, X_2, and X_3 represent the drum speed, flexible body thickness, and rod tooth length, respectively. Y_1, Y_2, and Y_3 represent the crushing rate, entrainment loss rate, and uncleaned rate, respectively.

Table 4. Experimental factors of codes.

Code	Drum Speed X_1/(r·min^{-1})	Flexible Body Thickness X_2/(mm)	Rod Tooth Length X_3/(mm)
−1.682	650	2	50
−1	690	2.8	58.1
0	750	4	70
1	809	5.2	81.9
1.682	850	6	90

Table 5. Experiment design and results.

No.	Factor			Result		
	Drum Speed X_1/(r·min^{-1})	Flexible Body Thickness X_2/(mm)	Rod Tooth Length X_3/(mm)	Y_1/%	Y_2/%	Y_3/%
1	−1	−1	−1	1.92	1.90	3.21
2	1	−1	−1	2.14	3.40	0.92
3	−1	1	−1	1.45	1.40	1.95
4	1	1	−1	1.67	1.60	2.81
5	−1	−1	1	3.32	3.25	2.27
6	1	−1	1	1.54	3.60	0.61
7	−1	1	1	2.35	2.35	4.15
8	1	1	1	1.71	2.45	2.73
9	−1.682	0	0	0.97	1.25	4.71
10	1.682	0	0	1.35	4.15	0.74
11	0	−1.682	0	2.31	1.90	0.95
12	0	1.682	0	2.17	1.05	3.82

Table 5. *Cont.*

No.	Factor			Result		
	Drum Speed X_1/(r·min^{-1})	Flexible Body Thickness X_2/(mm)	Rod Tooth Length X_3/(mm)	Y_1/%	Y_2/%	Y_3/%
13	0	0	−1.682	2.22	1.10	2.84
14	0	0	1.682	1.24	4.35	0.92
15	0	0	0	0.77	1.35	1.97
16	0	0	0	1.19	1.45	2.22
17	0	0	0	1.55	0.75	2.17
18	0	0	0	2.53	1.25	1.95
19	0	0	0	0.81	0.80	1.86
20	0	0	0	3.40	1.70	1.63
21	0	0	0	1.54	1.95	1.45
22	0	0	0	2.38	1.30	1.85
23	0	0	0	3.11	1.40	1.61

Table 6. Variance analysis of regression equation.

Variance Source	Crushing Rate				Entrainment Loss Rate				Uncleaned Rate			
	Square Sum	Freedom Degree	F	*p*	Square Sum	Freedom Degree	F	*p*	Square Sum	Freedom Degree	F	*p*
Model	1906.13	9	27.06	<0.0001 **	449.14	9	10.85	0.0001 **	562.27	9	10.67	<0.0001 **
X_1	151.19	1	19.32	0.0005 **	17.54	1	3.81	0.0424 *	65.74	1	11.21	<0.0001 **
X_2	193.49	1	24.72	0.0011 **	32.92	1	7.16	0.0166 *	66.78	1	11.39	<0.0001 **
X_3	106.34	1	13.59	0.0028 **	15.64	1	19.46	0.0007 **	40.42	1	6.89	0.021 *
$X_{1\times2}$	12.01	1	1.53	0.2327	1.53	1	1.03	0.5738	4.96	1	0.85	0.3744
$X_{1\times3}$	47.04	1	6.01	0.0291 *	43.71	1	0.67	0.0087 **	0.061	1	0.01	0.9202
$X_{2\times3}$	11.05	1	1.41	0.234	3.78	1	0.027	0.3811	27.75	1	4.73	0.0486 *
X_1^2	360.07	1	46.01	<0.0001 **	70.64	1	14.3	0.0023 **	108.26	1	18.24	0.0017 **
X_2^2	468.86	1	59.91	<0.0001 **	93.58	1	0.35	0.0006 **	139.92	1	23.86	0.0097 **
X_3^2	574.97	1	73.47	<0.0001 **	174.15	1	14.80	0.0020 **	113.02	1	19.35	0.0007 **
Residual	13.90	5	0.25		15.51	5			14.67	5		
Lack of fit	87.84	8	2.03	0.1788	44.28	8	3.62	0.0534	61.42	8	3.39	0.0632
Error	2007.88	22			508.93	22			638.36	22		
Sum	1906.13	9	27.06		449.14	9			562.27	9		

Note: * significant (*p* < 0.05) and ** extremely significant (*p* < 0.01).

5.4. Establishment and Significance Testing of Regression Mathematical Models

Multiple regression fitting was performed on the experimental data using Design-Expert 8.0.6 software, and regression analysis was performed on the experimental results to obtain regression equations for crushing rate Y_1, entrainment loss rate Y_2, and uncleaned rate Y_3, respectively.

5.4.1. Crushing Rate Y_1

Through experiments and multiple regression fitting of experimental data, the regression model for the impact of various factors on crushing rate Y_1 is obtained as follows:

$$Y_1 = 91.42 + 3.33X_1 + 3.76X_2 + 2.79X_3 + 1.23X_1X_2 - 2.42X_1X_3 + 1.18X_2X_3 - 4.76X_1^2 - 5.43X_2^2 - 6.02X_3^2 \tag{18}$$

The regression model has a *p*-value less than 0.01, indicating a highly significant degree of fit. However, the values of the interaction term between drum speed and flexible body thickness ($X_{1\times2}$), as well as the interaction term between flexible body thickness and rod tooth length ($X_{2\times3}$), are greater than 0.05, indicating that the interaction term between drum speed and flexible body thickness, as well as the interaction term between flexible body thickness and rod tooth length, have no significant impact on the crushing rate. The *p*-value of the interaction term ($X_{1\times3}$) between drum speed and rod tooth length is greater than 0.01, indicating that both drum speed and rod tooth length have a significant impact on the crushing rate. For lack of fit, $p = 0.1788 > 0.05$. This indicates that the regression model fits well with the actual situation, and the equation can accurately reflect the relationship between the crushing rate and various factors, their interaction terms, and quadratic terms. Excluding insignificant factors, a new regression model is obtained as follows:

$$\begin{aligned} Y_1 = {} & 132.63 + 3.33X_1 + 3.76X_2 + 2.79X_3 - 2.42X_1X_3 \\ & -5.23X_1{}^2 - 6.32X_2{}^2 - 6.42X_3{}^2 \end{aligned} \tag{19}$$

5.4.2. Entrainment Loss Rate Y_2

Through experiments and multiple regression fitting of experimental data, a regression model can be obtained for the influence of various factors on the entrainment loss rate Y_2:

$$\begin{aligned} Y_2 = {} & 4.17 - 1.13X_1 - 1.55X_2 - 1.07X_3 - 0.04X_1X_2 \\ & +2.34X_1X_3 + 0.69X_2X_3 + 2.11X_1{}^2 + 2.43X_2{}^2 + 3.31X_3{}^2 \end{aligned} \tag{20}$$

The regression model has a $p < 0.01$ and a highly significant degree of fit. However, the *p*-value of the interaction term between drum speed and flexible body thickness ($X_{1\times2}$), as well as the interaction term between flexible body thickness and rod tooth length ($X_{2\times3}$), is greater than 0.05, indicating that the interaction term between drum speed and flexible body thickness, as well as the interaction term between flexible body thickness and rod tooth length, does not have a significant impact on the entrainment loss rate. The impact of other factors on the entrainment loss rate is significant. For lack of fit, $p = 0.0534 > 0.05$, indicating that the regression model fits well with the actual situation. The equation can correctly reflect the relationship between entrainment loss rate and various factors, their interaction terms, and quadratic terms. Excluding insignificant factors, a new regression model is obtained as follows:

$$\begin{aligned} Y_2 = {} & 5.25 - 1.13X_1 - 1.55X_2 - 1.07X_3 \\ & +2.34X_1X_3 + 2.52X_1{}^2 + 2.85X_2{}^2 + 3.17X_3{}^2 \end{aligned} \tag{21}$$

5.4.3. Uncleaned Rate

Through experiments and multiple regression fitting of experimental data, a regression model can be obtained for the impact of various factors on the uncleaned rate Y_3:

$$\begin{aligned} Y_3 = {} & 4.52 - 2.19X_1 - 2.21X_2 - 1.72X_3 - 0.79X_1X_2 + 0.088X_1X_3 \\ & -1.86X_2X_3 + 2.61X_1{}^2 + 2.97X_2{}^2 + 2.66X_3{}^2 \end{aligned} \tag{22}$$

The regression model has a $p < 0.01$ and a highly significant degree of fit. However, the *p*-values of the interaction term between drum speed and flexible body thickness ($X_{1\times2}$), as well as the interaction term between drum speed and rod tooth length ($X_{1\times3}$), are greater than 0.05, indicating that the interaction term between drum speed and flexible body thickness, as well as the interaction term between drum speed and rod tooth length, has no significant impact on the uncleaning rate. The other factors have a significant impact on the uncleaning rate. For lack of fit, $p = 0.0632 > 0.05$, indicating that the regression model fits well with the actual situation. The equation can correctly reflect the relationship

between the uncleaning rate and various factors, their interaction terms, and quadratic terms. Excluding insignificant factors, a new regression model is obtained as follows:

$$Y_3 = 5.04 - 2.19X_1 - 2.21X_2 - 1.72X_3 \\ -1.86X_2X_3 + 3.05X_1{}^2 + 3.14X_2{}^2 + 2.96X_3{}^2 \tag{23}$$

5.5. Factor Response Surface Analysis

According to Figure 16a, the crushing rate increases with the increase in drum speed, and there is a quadratic relationship between the crushing rate and drum speed. It can be inferred that the crushing rate is proportional to the square of the collision speed, and the essence of grain loss caused by the collision between ratoon rice grains and rod teeth should be the conversion of the kinetic energy of ratoon rice grains into other forms of energy. The crushing rate first decreases and then increases with the increase in the rod tooth length; it reaches its lowest point when the length of the rod tooth is around 70 mm.

(**a**) (**b**) (**c**)
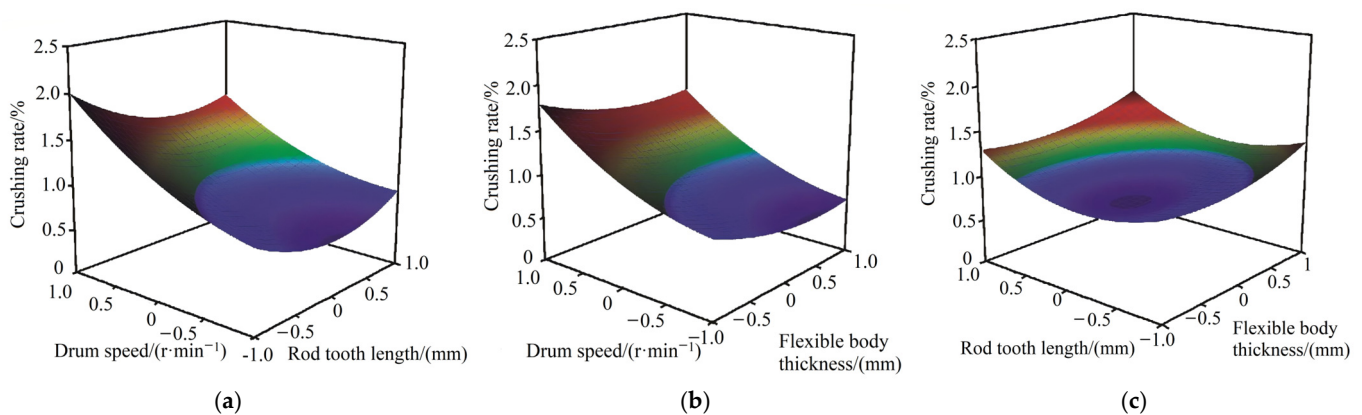
Figure 16. Effects of interactive factors on the crushing rate. (**a**) The interaction between drum speed and rod tooth length. (**b**) The interaction between drum speed and flexible body thickness. (**c**) The interaction between rod tooth length and flexible body thickness.

According to Figure 16b, the relationship between the crushing rate and the drum speed follows a quadratic curve. As the drum speed increases, the crushing rate increases rapidly. The relationship between the crushing rate and the thickness of the flexible body follows a quadratic curve. When the thickness of the flexible body is 2–4 mm, the crushing rate rapidly decreases with the increase in the thickness of the flexible body. When the thickness of the flexible body is 4–6 mm, the crushing rate slowly decreases with the increase in the thickness of the flexible body.

According to Figure 16c, without considering the influence of the thickness of the flexible body, when the crushing rate is at its lowest, the length of the rod teeth is around 70 mm. Without considering the influence of tooth length, when the crushing rate is at its lowest, the thickness of the flexible body is about 4 mm.

5.6. Optimal Parameters

The experimental results were optimized using Design-Expert (8.0.6) software, and the results showed that when the rod tooth length, drum speed, and flexible body thickness were 72.7 mm, 684 r/min, and 3.86 mm, respectively, the crushing rate, entrainment loss rate, and uncleaning rate were 1.260%, 2.132%, and 1.241%, respectively.

The distribution of regenerated rice grains shown in the bench test is consistent with the phenomenon observed in Section 4.3.2 of this article, which proves that the simulation parameter settings are accurate and that the simulation is effective. To verify the best results, the experiment was repeated three times, and the obtained results were compared with those of a conventional threshing system, as shown in Table 7. In simulation analysis, the entrainment loss rate is calculated by the difference between the total weight of the

ratoon rice grains that were fed into the thresher and the weight of the ratoon rice grains in the collection box below. To calculate the crushing rate, we randomly selected ratoon rice grains, obtained their peak stress values during the simulation process, and determined whether they were broken based on the peak stress values. The results in Table 7 indicate that the rigid–flexible coupling rod teeth designed in our research have the ability to reduce the crushing of ratoon rice, which helps to improve the economic benefits of ratoon rice. At the same time, the distribution of ratoon rice and short straw in the material boxes below the threshing drum was statistically analyzed and compared with the simulation results. It was found that the distribution of the two was consistent, proving the effectiveness of using MBD–DEM to simulate the threshing process of ratoon rice. The reason for the difference between the simulation results and the bench test is that the mixture during the bench test contains components such as rice leaves and weeds, which makes the various indicators biased; however, the difference is small.

Table 7. Comparative analysis of results.

| Item | Simulation Result | Bench Test (Ratoon Rice) | | Change Rate/% |
		Rigid–Flexible Coupling Threshing Device (After Parameter Optimization)	Traditional Threshing Device	
Crushing rate/%	1.132	1.260	2.842	55.7
Entrainment loss rate/%	1.963	2.132	2.943	27.5
Uncleaning rate/%	1.114	1.237	2.482	50.2

6. Conclusions

(1) Through the analysis of the force and collision model of ratoon rice grains, it was confirmed that changing the structural parameters and the materials that cover the surface of the threshing rod teeth can reduce the peak collision force. Therefore, a design scheme for reducing the loss of ratoon rice grains through rigid–flexible coupling rod teeth was proposed, and structural design and parameter calculations were carried out for key components of the threshing device.

(2) Using MBD–DEM coupling to simulate the threshing process of ratoon rice, it was found that the main component affecting the grain crushing rate of ratoon rice is the rod teeth. As the feeding amount increases, the impact force on the rod teeth continues to increase. When the feeding amount exceeds 5.0 kg/s, the increase in impact force weakens. As the thickness of the flexible body increases, the impact force on the teeth decreases continuously. When the thickness of the flexible body is 8 mm, the impact force on the teeth reaches its lowest point, and the fluctuation in the impact force is minimal. However, at this time, the threshing effect of the teeth is the weakest.

(3) A three-factor quadratic regression orthogonal rotation combination experiment was conducted with drum speed, flexible body thickness, and rod tooth length as experimental factors. The results showed that when the drum speed was 684 r/min, the flexible body thickness was 3.86 mm, the rod tooth length was 72.7 mm, the crushing rate was 1.260%, the entrainment loss rate was 2.132%, and the uncleaned rate was 1.241%. Compared with traditional threshing devices, the crushing rate, entrainment loss rate, and uncleaning rate of the rigid–flexible coupling rod tooth threshing device were reduced by 55.7%, 27.5%, and 50.2%, respectively, indicating that this structure has a significant effect on reducing grain loss and improving economic benefits.

References

1. Zhao, Z.; Huang, H.; Yin, J.; Yang, S. Dynamic analysis and reliability design of round baler feeding device for rice straw harvest. *Biosyst. Eng.* **2018**, *174*, 10–19. [CrossRef]
2. Xing, S.; Yu, Y.; Cao, G.; Hu, J.; Zhu, L.; Liu, J.; Wu, Q.; Li, Q.; Xu, L. Design and Parametric Optimization Study of an Eccentric Parallelogram-Type Uprighting Device for Ratoon Rice Stubbles. *Agriculture* **2024**, *14*, 534. [CrossRef]
3. Liu, W.; Zeng, S.; Chen, X. Design and experiment of spiral step cleaning device for ratooning rice based on CFD-DEM coupling. *Comput. Electron. Agric.* **2024**, *224*, 109207. [CrossRef]
4. Liu, W.; Luo, X.; Zeng, S.; Wen, Z. Numerical simulation and experiment of grain motion in the conveying system of ratooning rice harvesting machine. *Int. J. Agric. Biol. Eng.* **2022**, *15*, 103–115. [CrossRef]
5. Liu, W.; Luo, X.; Zeng, S. The Design and Test of the Chassis of a Triangular Crawler-Type Ratooning Rice Harvester. *Agriculture* **2022**, *12*, 890. [CrossRef]
6. Liu, W.; Luo, X.; Zeng, S. Performance test and analysis of the self-adaptive profiling header for ratooning rice based on fuzzy PID control. *Trans. Chin. Soc. Agric. Eng.* **2022**, *38*, 1–9.
7. Liu, W.; Zeng, S.; Chen, X. Design and Experiment of Adaptive Profiling Header Based on MultiBody Dynamics–Discrete Element Method Coupling. *Agriculture* **2024**, *14*, 105. [CrossRef]
8. Wang, J.; Guo, F.; Xu, Y.; Zhu, J.; Li, R.; Tang, H.; Zhou, W.; Wang, Q.; Sun, X. Analysis of the Interaction Mechanism between Preharvest Threshing Device and Rice at Harvesting Period Based on DEM Simulations and Bench Tests. *Agriculture* **2024**, *14*, 183. [CrossRef]
9. Ma, L.; Xie, F.; Liu, D.; Wang, X.; Zhang, Z. An Application of Artificial Neural Network for Predicting Threshing Performance in a Flexible Threshing Device. *Agriculture* **2023**, *13*, 788. [CrossRef]
10. Hao, S.; Tang, Z.; Guo, S.; Ding, Z.; Su, Z. Model and Method of Fault Signal Diagnosis for Blockage and Slippage of Rice Threshing Drum. *Agriculture* **2022**, *12*, 1968. [CrossRef]
11. Xu, L.; Li, Y.; Ding, L. Contacting mechanics analysis during impact process between rice and threshing component. *Trans. Chin. Soc. Agric. Eng.* **2008**, *24*, 146–149.
12. Xu, L.; Li, Y. Critical Speed of Impact Damage on a Rice Kernel. *Trans. Chin. Soc. Agric. Mach.* **2009**, *40*, 54–57.
13. Liu, Y.; Li, Y.; Dong, Y.; Huang, M.; Zhang, T.; Cheng, J. Development of a variable-diameter threshing drum for rice combine harvester using MBD—DEM coupling simulation. *Comput. Electron. Agric.* **2022**, *196*, 106859. [CrossRef]
14. Wang, X.; Li, Y.; Xu, L. Relationship between thresher velocities and rice grain broken rate. *Trans. Chin. Soc. Agric. Eng.* **2007**, *23*, 16–19. [CrossRef]
15. Xie, F.; Luo, X.; Lu, X. Threshing principle of flexible pole-teeth roller for paddy rice. *Trans. Chin. Soc. Agric. Eng.* **2009**, *25*, 110–114.
16. Fu, Q.; Fu, J.; Wang, F.; Chen, Z.; Ren, L. Design and parameter optimization of corn head with wheel type rigid-flexible coupling snapping device to reduce loss. *Trans. Chin. Soc. Agric. Eng.* **2019**, *35*, 21–30.
17. Miu, P.; Kutzbach, H. Modeling and simulation of grain threshing and separation in threshing units-Part I. *Comput. Electron. Agric.* **2008**, *60*, 96–104. [CrossRef]
18. Trollope, J. A mathematical model of the threshing process in a conventional combine-thresher. *J. Agr. Eng. Res.* **1982**, *27*, 119–130. [CrossRef]
19. Wang, Q.; Mao, H.; Li, Q. Modelling and simulation of the grain threshing process based on the discrete element method. *Comput. Electron. Agric.* **2020**, *178*, 105790. [CrossRef]
20. China Academy of Agricultural Mechanization Sciences. *Agricultural Machinery Design Manual*; China Agricultural Science Technology Press: Beijing, China, 2007; pp. 928–933.
21. Wang, L.; Peng, B.; Song, H. Cleaning of Maize Mixture Based on Polyurethane Rubber Sieve. *Trans. Chin. Soc. Agric. Mach.* **2018**, *49*, 90–96.
22. Gao, X.; Xie, G.; Xu, Y. Application of a staggered symmetrical spiral groove wheel on a quantitative feeding device and investigation of particle motion characteristics based on DEM. *Powder Technol.* **2022**, *407*, 117650. [CrossRef]

23. Gao, X.; Zhou, Z.; Xu, Y. Numerical simulation of particle motion characteristics in a quantitative seed feeding system. *Powder Technol.* **2020**, *367*, 643–658. [CrossRef]
24. Gao, X.; Cui, T.; Zhou, Z. DEM study of particle motion in a novel high-speed seed metering device. *Adv. Powder Technol.* **2021**, *32*, 1438–1449. [CrossRef]
25. Zhan, S.; Li, Y.; Dong, Y. Simulation of rice threshing performance with concentric and non-concent-ric threshing gaps. *Biosyst. Eng.* **2020**, *197*, 270–284.
26. Li, X.; Du, Y.; Liu, L. Research on the constitutive model of low-damage corn threshing based on DEM. *Comput. Electron. Agric.* **2022**, *194*, 106722. [CrossRef]